

StitchFusion: Weaving Any Visual Modalities to Enhance Multimodal Semantic Segmentation

Bingyu Li^{1,3*}, Da Zhang^{2,3*}, Zhiyuan Zhao³, Junyu Gao^{2,3}, Xuelong Li^{3†}

¹Department of Electronic Engineering and Information Science, University of Science and Technology of China, China

²School of Artificial Intelligence, OPtics and ElectroNics (iOPEN), Northwestern Polytechnical University, China

³Institute of Artificial Intelligence (TeleAI), China

libingyu0205@mail.ustc.edu.cn, dazhang@mail.nwpu.edu.cn, tuzixini@163.com,
gjy3035@gmail.com, xuelong_li@ieee.org

Abstract

Multimodal semantic segmentation shows significant potential for enhancing segmentation accuracy in complex scenes. However, current methods often incorporate specialized feature fusion modules tailored to specific modalities, thereby restricting input flexibility and increasing the number of training parameters. To address these challenges, we propose *StitchFusion*, a straightforward yet effective modal fusion framework that integrates large-scale pre-trained models directly as encoders and feature fusers. This approach facilitates comprehensive multi-modal and multi-scale feature fusion, accommodating any visual modal inputs. Specifically, Our framework achieves modal integration during encoding by sharing multi-modal visual information. To enhance information exchange across modalities, we introduce a multi-directional adapter module (*MultiAdapter*) to enable cross-modal information transfer during encoding. By leveraging *MultiAdapter* to propagate multi-scale information across pre-trained encoders during the encoding process, *StitchFusion* achieves multi-modal visual information integration during encoding. Extensive comparative experiments demonstrate that our model achieves state-of-the-art performance on four multi-modal segmentation datasets with minimal additional parameters. Furthermore, the experimental integration of *MultiAdapter* with existing Feature Fusion Modules (FFMs) highlights their complementary nature. Our code is available at [StitchFusion_repo](#).

Introduction

Semantic segmentation is a critical vision processing technique extensively applied in scene understanding, change detection, and autonomous driving (Chen et al. 2017). This technique enables systems to accurately recognize and interpret the surrounding environment by analyzing the semantic information of each image pixel (Chen et al. 2018). Given its importance and wide range of applications, numerous researchers have focused on semantic segmentation tasks and achieved significant results with models such as FCN (Long, Shelhamer, and Darrell 2015), and Deeplab (Chen et al. 2021). Despite the success of these models, most related research has primarily focused on single visual fea-

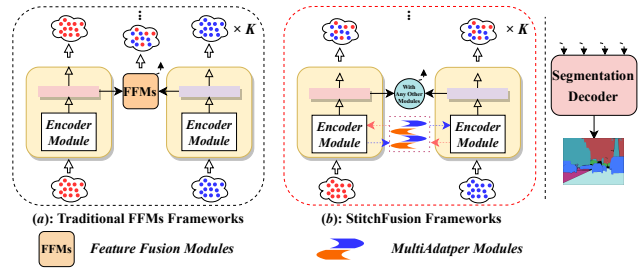


Figure 1: Comparison of different model fusion paradigms. (a) illustrates the design of the traditional FFMs to map features into the same subspace for feature fusion, while our method (b) utilizes the pre-trained model as the encoder and feature fusion module by *StitchFusion* framework which can complement any other FFMs. Red and blue points represent information from different modalities, respectively.

tures (RGB), limiting their effectiveness in complex scenes and special environments, such as nighttime.

As application demands increase, processing a single modality is no longer sufficient to meet the requirements (He 2024). Consequently, the community is increasingly focusing on multimodal semantic segmentation (Jozé et al. 2020). Unlike traditional segmentation tasks that rely solely on RGB modalities, multimodal semantic segmentation leverages the complementary features of multiple visual modalities. Each modality can provide unique information: RGB captures color and texture, TIR captures thermal properties useful in low-light conditions, and depth sensors provide spatial and structural information (Zhang et al. 2023a). By fusing these complementary modalities, segmentation models can achieve higher accuracy and robustness. This approach improves the limitations of a single modality in challenging scenes and enhances the ability to capture scene-specific features.

Given the complementary nature of multimodal information, achieving the effective fusion of multiple visual modalities is crucial. Previous researchers have designed numerous feature fusion modules (Zhang et al. 2023a; Fu et al. 2019), the framework can be summarized as Fig. 1(a). Essentially, these methods remap features extracted by en-

*These authors contributed equally.

†Corresponding author

coders into a new subspace to achieve modality fusion (Zhou et al. 2023). Although these methods have achieved certain levels of effectiveness, they typically encounter the following two limitations: 1) the complexity of feature extraction and fusion modules introduces a large number of additional parameters, thereby increasing training costs; and 2) existing FFMs are designed for specific modalities, and thus, are not effective for arbitrary modality combinations.

These limitations prompt us to rethink the design and training of an effective multimodal fusion layer to address the aforementioned problems. Given the extensive generalizability and capability of pre-trained encoders to capture both global and local vision features, much-related work utilizes pre-trained models as feature extractors (Zhang et al. 2023a; Chen et al. 2017). However, the potential of these pre-trained models as feature fusion models for semantic segmentation remains underexplored.

Inspired by these considerations, we propose a new feature fusion paradigm (*StitchFusion*) that utilizes pre-trained models as a feature fusion layer to demonstrate potential benefits. To achieve this target, we employ a simple Multidirectional MLP layer, named *MultiAdapter*, which shares and synchronizes modality-specific multi-scale information throughout the encoding process. This *MultiAdapter* ensures effective feature fusion during encoding, as illustrated in Fig. 1(b). This method leverages the encoder’s inherent multi-scale visual feature modeling capabilities, requiring fewer additional parameters for cross-modal fusion. Experimental results on 4 datasets confirm that this new fusion paradigm not only outperforms traditional feature fusion methods but also enhances segmentation efficacy when combined.

Our contributions are summarized as follows:

- We introduce a multimodal feature fusion framework called *StitchFusion*, which achieves cross-modal integration by enabling modality sharing during the encoding process.
- We designed a multidirectional MLP layer called *Multi-Adapter*, which enables cross-modal information sharing. By this, our framework leverages the encoder’s feature extraction capabilities to achieve effective feature fusion.
- Experiments on various multimodal semantic segmentation datasets with the *StitchFusion* module for ViT-based encoder surpass previous state-of-the-art results. Comprehensive ablation studies suggest potential optimal placements and quantities for integrating the *StitchFusion* module to maximize modal fusion efficacy.
- The *StitchFusion* module and existing approaches based on additional FFMs can complement each other in terms of design and application, and we demonstrate their complementary nature through extensive experiments.

Related Work

Semantic Segmentation

Semantic segmentation, a critical task in computer vision, has evolved significantly by developing various methods

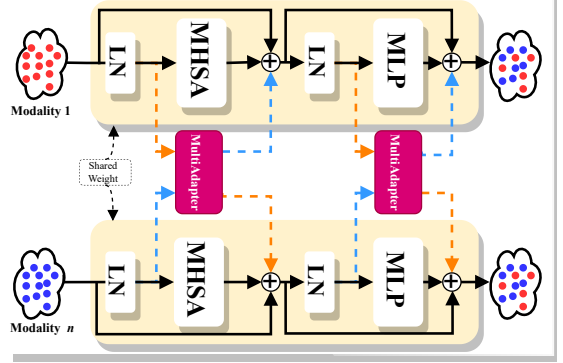


Figure 2: StitchFusion Framework With ViT Encoder.

and models, particularly those leveraging convolutional neural networks (CNNs) and more recently, transformers (Xie et al. 2021). Early breakthroughs were achieved through fully convolutional networks (FCNs) (Long, Shelhamer, and Darrell 2015), which enabled end-to-end pixel-wise predictions. Subsequent architectures, such as SegNet (Badri-narayanan, Kendall, and Cipolla 2017) and U-Net (Ronneberger, Fischer, and Brox 2015), utilized encoder-decoder structures to capture both low-level and high-level features. The DeepLab series (Chen et al. 2017, 2018) introduced atrous convolutions and spatial pyramid pooling to enhance multi-scale context perception, while PSPNet (Zhao et al. 2017) aggregated context from different regions. Vision Transformer (ViT) models (Dosovitskiy et al. 2020) leveraged self-attention mechanisms to capture long-range dependencies, with subsequent adaptations like SETR (Zheng et al. 2021) and Swin Transformer (Liu et al. 2021) improving computational efficiency and scalability. While single-modality data has seen substantial progress, multimodal semantic segmentation, integrating data such as RGB with other vision modalities, has been increasingly explored. The existing literature has proposed numerous feature fusion approaches (Hazirbas et al. 2016). Building on these advancements, we propose the *StitchFusion* model which introduces a novel feature fusion paradigm (*StitchFusion*) using Multidirectional MLP layer (*MultiAdapter*) for effective multimodal integration.

Vision Multimodal Fusion

In classical visual tasks, single visual modalities often struggle to handle challenges in complex environments adaptively (Fu et al. 2019; Zhang et al. 2023a). Consequently, an increasing number of researchers are turning to multiple visual modalities, making the fusion of these modalities crucial. Some researchers have used fine-tuned pre-trained models to fuse multiple visual modalities, but this approach can lead to catastrophic forgetting. To mitigate this problem, many researchers have opted to freeze the pre-trained models, as seen in the work (He 2024; Cao et al. 2024) proposing a prompt-based method for multimodal fusion. Another paradigm utilizes multi-scale information and designs various FFMs to integrate the multi-scale information from each

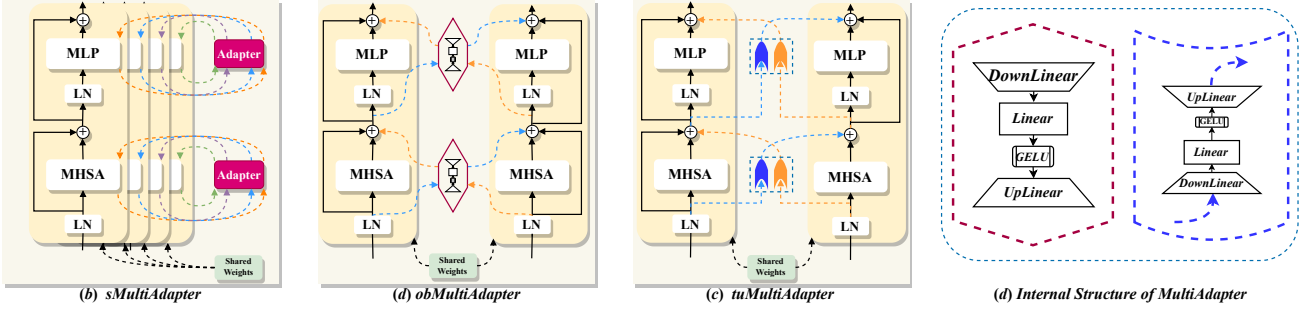


Figure 3: MultiAdapter Module At Different Density Levels. (a) Shared MultiAdapter for All Modalities (*sMultiAdapter*). (b) Independent MultiAdapter for Each Pair of Modalities (*obMultiAdapter*). (c) Parallel MultiAdapters for Each Pair of Modalities (*tuMultiAdapter*). (d) A feasible internal structure of the MultiAdapter.

modality (Zhang et al. 2023b; Dong et al. 2023; Huang et al. 2019). Although existing FFMs have achieved notable experimental results, they introduce excessive additional parameters and are often limited in the number of modality data they can handle. Therefore, in this paper, we introduce *StitchFusion*, a simple but effective feature fusion framework incorporating the plug-and-play *MultiAdapter* module, which enables modality sharing with fewer parameters, thereby achieving feature fusion during the encoding process.

Method

This section introduces a new multimodal feature fusion framework for semantic segmentation, named *StitchFusion*. Furthermore, we propose a multidirectional Adapter for cross-modal information sharing.

Feature Extraction And Encoding

Unlike traditional CNNs that often struggle to capture long-range dependencies within images, we chose SegFormer (Xie et al. 2021) as our frozen feature encoder in this paper. SegFormer is based on the Vision Transformer (ViT) architecture. Its self-attention layers provide a comprehensive view of the input data. Integrating a Feature Pyramid Network (FPN) within SegFormer’s architecture further enhances its ability to discern multi-scale features, ensuring that fine-grained details and broader contextual features are effectively encoded. The model’s end-to-end training approach eliminates the need for post-processing steps and allows for a seamless transition from raw image data to precise features, which makes it effective for our feature fusion.

Based on SegFormer’s ViT architecture, we devise the *StitchFusion* framework by viewing the ViT block as the encoder and feature fuser shown in Fig. 2.

StitchFusion Framework

We employ the MultiAdapter Layer as an information exchanger for the ViT encoder to enable the frozen pre-trained model to function as a modality fuser. The specific data flow process is as follows.

The attention mechanism independently processes input feature map \mathbf{x}_i of i -th modality. This step leverages the self-attention mechanism F^{Attn} to capture dependencies and relationships within the feature map \mathbf{x}_i of i -th modality:

$$\mathbf{z}_i^{Attn} = \mathbf{x}_i + \text{DropPath}(F^{Attn}(LN_1(\mathbf{x}_i))). \quad (1)$$

The MultiAdapter F^{Ada_1} is then used to influence the feature maps between the i -th and the j -th modalities, which allows information to flow from one modality to another:

$$\mathbf{z}_j^{Attn} = \mathbf{z}_j^{Attn} + \text{DropPath}(F^{Ada_1}(LN_1(\mathbf{x}_i))), \quad (2)$$

for $i \neq j$. Subsequently, each input is independently processed through the F^{MLP} . This processing step involves non-linear transformations that further refine the features, preparing them for subsequent stages of the model:

$$\mathbf{z}_i^{MLP} = \mathbf{z}_i^{Attn} + \text{DropPath}(F^{MLP}(LN_2(\mathbf{z}_i^{Attn}))). \quad (3)$$

The MultiAdapter F^{Ada_2} is then applied again for the final cross-modal influence.

$$\mathbf{z}_j^{MLP} = \mathbf{z}_j^{MLP} + \text{DropPath}(F^{Ada_2}(LN_2(\mathbf{z}_i^{Attn}))), \quad (4)$$

for $i \neq j$. This second application of the MultiAdapter ensures that the refined features from different modalities are effectively integrated.

The specific structure and the sequence of operations are illustrated in Fig. 2, which provides a visual representation of the *StitchFusion* framework.

MultiAdapter

we design a simple *MultiAdapter* F^{Ada} based on the linear module which performs the following operations during the information-sharing process: Downscaling, Processing and Upscaling.

Mathematically, these operations are defined as follows: Given an input feature vector $\mathbf{x} \in \mathbb{R}^d$, the downscaling transformation is defined as:

$$\mathbf{x}_{\text{down}} = \mathbf{W}_{\text{down}} \mathbf{x} + \mathbf{b}_{\text{down}}, \quad (5)$$

where $\mathbf{W}_{\text{down}} \in \mathbb{R}^{d \times r}$ is the weight matrix and $\mathbf{b}_{\text{down}} \in \mathbb{R}^{d \times r}$ is the bias vector.

The downscaled features are then processed using a non-linear activation function (GELU) and dropout regularization:

$$\mathbf{x}_{\text{mid}} = \text{Dropout}(\text{GELU}(\mathbf{W}_{\text{mid}} \mathbf{x}_{\text{down}} + \mathbf{b}_{\text{mid}})), \quad (6)$$

where $\mathbf{W}_{\text{mid}} \in \mathbb{R}^{r \times r}$ is the weight matrix and $\mathbf{b}_{\text{mid}} \in \mathbb{R}^{r \times r}$ is the bias vector.

Finally, the processed features are upscaled back to the original dimension:

$$\mathbf{x}_{\text{up}} = \mathbf{W}_{\text{up}} \mathbf{x}_{\text{mid}} + \mathbf{b}_{\text{up}}, \quad (7)$$

where $\mathbf{W}_{\text{up}} \in \mathbb{R}^{r \times d}$ is the weight matrix and $\mathbf{b}_{\text{up}} \in \mathbb{R}^{r \times d}$ is the bias vector.

MultiAdapter At Different Density Levels

This section extends the concept to support multiple modalities and different levels of connection density, providing a detailed analysis of various configurations and their implications for model performance.

Shared MultiAdapter for All Modalities. In this configuration (Fig. 3(a)), all modalities share the same MultiAdapter (named *sMultiAdapter*). This means that the same set of weights and biases are used for the transformations between any pair of modalities. This approach promotes consistency and reduces the overall number of parameters, making the model more efficient and easier to train. The transformation for any modality pair (i, j) uses the same weights and biases:

$$\mathbf{y}_{i \rightarrow j} = \mathbf{W}_{\text{shared}} \mathbf{x}_i + \mathbf{b}_{\text{shared}}, \quad (8)$$

$$\mathbf{y}_{j \rightarrow i} = \mathbf{W}_{\text{shared}} \mathbf{x}_j + \mathbf{b}_{\text{shared}}. \quad (9)$$

Using a shared set of weights, the *sMultiAdapter* ensures that the transformations are uniform across all modality pairs, which can be beneficial in scenarios where the modalities have similar feature distributions.

Independent MultiAdapter for Each Pair of Modalities. In this configuration (Fig. 3(b)), each pair of modalities has its own bi-directional MultiAdapters (named *obMultiAdapter*). For M modalities, there are C_M^2 MultiAdapters in total, where each pair of modalities (i, j) is assigned a unique set of weight matrices and biases. Let \mathbf{x}_i and \mathbf{x}_j be the feature vectors for modalities i and j respectively, the transformation is defined as:

$$\mathbf{y}_{i \rightarrow j} = \mathbf{W}_{i \rightarrow j} \mathbf{x}_i + \mathbf{b}_{i \rightarrow j}, \quad (10)$$

$$\mathbf{y}_{j \rightarrow i} = \mathbf{W}_{j \rightarrow i} \mathbf{x}_j + \mathbf{b}_{j \rightarrow i}. \quad (11)$$

Each pair (i, j) has a unique set of weight matrices and biases. This configuration allows for more specialized transformations tailored to the specific characteristics of each modality pair. This is especially useful when the modalities have significantly different feature distributions, as it allows for more precise adaptations.

Parallel MultiAdapters for Each Pair of Modalities. In this configuration (Fig. 3(c)), each pair of modalities shares two uni-directional MultiAdapter Modules (named *tuMultiAdapter*). This means that there are separate weight matrices and biases for the transformations in each direction between two modalities, allowing for asymmetric information exchange. The transformation is:

$$\mathbf{y}_{i \rightarrow j} = \mathbf{W}_{i \rightarrow j} \mathbf{x}_i + \mathbf{b}_{i \rightarrow j}, \quad (12)$$

$$\mathbf{y}_{j \rightarrow i} = \mathbf{W}_{j \rightarrow i} \mathbf{x}_j + \mathbf{b}_{j \rightarrow i}, \quad (13)$$

where each pair (i, j) has a shared set of weight matrices and biases. This setup can capture directional dependencies and interactions more effectively, as it can learn distinct transformations for each direction.

Equivalence of Configurations for Two Modalities.

When the number of modalities $M = 2$, the configurations of a *sMultiAdapter* and an *obMultiAdapter* are equivalent. In both cases, the transformation involves a single set of weights and biases:

$$\mathbf{y}_{1 \rightarrow 2} = \mathbf{W} \mathbf{x}_1 + \mathbf{b}, \quad (14)$$

$$\mathbf{y}_{2 \rightarrow 1} = \mathbf{W} \mathbf{x}_2 + \mathbf{b}. \quad (15)$$

Thus, for $M = 2$:

$$\mathbf{W}_{1 \leftrightarrow 2} = \mathbf{W}_{\text{shared}}, \quad \mathbf{b}_{1 \leftrightarrow 2} = \mathbf{b}_{\text{shared}}. \quad (16)$$

In the remainder of the text, we will refer to the framework using *sMultiAdapter* as *sStitchFusion*, the framework using *obMultiAdapter* as *obStitchFusion*, and the framework using *tuMultiAdapter* as *tuStitchFusion*. Each of these frameworks offers distinct advantages depending on the number of modalities and the specific requirements of the application, providing flexible options for multimodal integration.

Experimental Result

Experimental Details

We test our model on 5 datasets. The FFMs in the paper is configed as the module from (Kaykobad and et al. 2023). We set the intermediate dimention for MultiAdatper to $r = 8$. the learning rate is 1.2×10^{-4} for the FMB dataset and 6×10^{-5} for others. Furthermore, a warm-up technology is implemented for the initial 10 epochs, followed by a learning rate decay factor of 0.01. For additional training details, please refer to the code implementation.

DataSet

MCubeS Dataset. (Liang et al. 2022) The MCubeS dataset includes RGB, Near-Infrared (NIR), Degree of Linear Polarization (DoLP), and Angle of Linear Polarization (AoLP) image pairs for semantic material segmentation across 20 categories. It consists of 302/96/102 image pairs for training/validation/testing, all sized at 1024×1024.

FMB Dataset. (Liu et al. 2023) The FMB dataset is designed for image fusion and segmentation, containing 1,500 infrared and visible image pairs annotated with 15 pixel-level categories. The training set has 1,220 pairs, and the test set has 280 pairs.

MFNet Dataset. (Ha et al. 2017) The MFNet dataset consists of 1,569 RGB-Thermal image pairs (640×480 pixels) with 8 classes. It includes 820 daytime and 749 nighttime image pairs.

DeLiVER Dataset. (Zhang et al. 2023b) The DeLiVER dataset includes six orthogonal views with data from Depth, LiDAR, Views, Event, and RGB sensors (1024×1024 pixels). DeLiVER contains 47,310 frames, with 7,885 annotated front-view samples.

PST900 Dataset. (Shivakumar et al. 2020) The PST900 dataset contains 894 synchronized RGB-Thermal image pairs with per-pixel ground truth annotations for five classes, divided into training and test sets.

Experimental Results on Datasets

Results On McubeS Dataset. In the MCubeS dataset (Table 1, the StitchFusion models demonstrate superior performance across different modality combinations. The highest mIoU of 53.92% is achieved by StitchFusion+FFMs using RGB-A-D-N modalities. The models consistently outperform other methods, showcasing the effectiveness of the StitchFusion approach in integrating multiple visual modalities to enhance segmentation accuracy. The improvements are significant across various combinations such as RGB-N, RGB-D, and RGB-A, highlighting the robustness and adaptability of the proposed method.

Methods	Modalities	mIoU (%)
StitchFusion	RGB-N	51.67
StitchFusion+FFMs	RGB-N	53.21
StitchFusion	RGB-D	51.25
StitchFusion+FFMs	RGB-D	52.72
MCubeSNet	RGB-A	39.10
CMNeXt	RGB-A	48.42
MMSFormer	RGB-A	51.30
StitchFusion	RGB-A	52.08 (+0.78)
StitchFusion+FFMs	RGB-A	52.68 (+1.38)
MCubeSNet	RGB-A-D	42.00
CMNeXt	RGB-A-D	49.48
MMSFormer	RGB-A-D	52.05
StitchFusion	RGB-A-D	52.52 (+0.47)
StitchFusion+FFMs	RGB-A-D	53.26 (+0.67)
MCubeSNet	RGB-A-D-N	42.86
CMNeXt	RGB-A-D-N	51.54
MMSFormer	RGB-A-D-N	53.11
StitchFusion	RGB-A-D-N	51.74
StitchFusion+FFMs	RGB-A-D-N	53.92 (+0.81)

Table 1: Comparison With State-of-the-art Results on MCubeS.

Results On DeLiVER Dataset. The comparative analysis of semantic segmentation methods on the DeLiVER dataset reveals that StitchFusion consistently outperforms its counterparts across various modalities (Table 2. With a notable 2.12% increase in mIoU over CMNeXt in RGB-Depth, and

an impressive 1.88% lead in the comprehensive RGB-DEL setup, StitchFusion demonstrates its robust feature integration capabilities. Particularly striking is its 1.15% improvement in the challenging RGB-D-LiDAR modality, showcasing its adept handling of multimodality data. These results underscore StitchFusion’s potential as a leading approach in the realm of advanced image segmentation.

Methods	Modalities	mIoU(%)
HRFuser	RGB-Depth	51.88
TokenFusion	RGB-Depth	60.25
CMX	RGB-Depth	62.67
CMNeXt	RGB-Depth	63.58
StitchFusion	RGB-Depth	65.75 (+2.12)
HRFuser	RGB-Event	42.22
TokenFusion	RGB-Event	45.63
CMX	RGB-Event	56.52
CMNeXt	RGB-Event	57.48
StitchFusion	RGB-Event	57.44 (-0.04)
HRFuser	RGB-LiDAR	43.13
TokenFusion	RGB-LiDAR	53.01
CMX	RGB-LiDAR	56.37
CMNeXt	RGB-LiDAR	58.04
StitchFusion	RGB-LiDAR	58.03 (-0.01)
HRFuser	RGB-D-Event	51.83
CMNeXt	RGB-D-Event	64.44
StitchFusion	RGB-D-Event	66.03 (+1.59)
HRFuser	RGB-D-LiDAR	52.72
CMNeXt	RGB-D-LiDAR	65.50
StitchFusion	RGB-D-LiDAR	66.65 (+1.15)
HRFuser	RGB-D-E-L	52.97
CMNeXt	RGB-D-E-L	66.30
StitchFusion*	RGB-D-E-L	68.18 (+1.88)

Table 2: Comparison With State-of-the-art Results on DeLiVER. * denotes the MultiAdapter is used in the latter two stages.

Results On FMB Dataset. For the FMB dataset (Table 3, the StitchFusion models exhibit exceptional performance, with the StitchFusion+FFMs achieving the highest mIoU of 64.32%. This substantial improvement over other models, including GMNet(Zhou et al. 2021) and MMSFormer(Kaykobad and et al. 2023). The significant increase in segmentation accuracy demonstrates the effectiveness of the proposed fusion techniques in handling diverse and challenging visual environments. It is evident that combining StitchFusion with FFMs results in a higher mIoU than using either method alone, highlighting the complementary nature of StitchFusion and FFMs.

Results On MFNet Dataset. In the MFNet dataset (Table 3(c)), the StitchFusion model variants continue to excel, with StitchFusion+FFMs achieving the highest mIoU of 57.91%. This performance surpasses other prominent models such as BiSeNet and SegHRNet, reinforcing the model’s generalizability and robustness in multimodal semantic segmentation tasks. The consistently high performance across multiple datasets indicates the versatility and effectiveness of the StitchFusion approach.

Methods	Modalities	mIoU (%)
FMB Dataset		
DiDFuse	RGB-Infrared	50.6
ReCoNet	RGB-Infrared	50.9
U2Fusion	RGB-Infrared	47.9
TarDAL	RGB-Infrared	48.1
SegMiF	RGB-Infrared	54.8
MMSFormer	RGB-Infrared	61.7
StitchFusion	RGB-Infrared	63.30 (+1.60)
StitchFusion+FFMs	RGB-Infrared	64.32 (+2.62)
MFNet Dataset		
GCFNet	RGB-Infrared	55.7
GEBNet	RGB-Infrared	56.2
GCGLNet	RGB-Infrared	55.4
DHFNet	RGB-Infrared	57.2
MDRNet++	RGB-Infrared	56.8
FDCNet	RGB-Infrared	56.3
EGFNet	RGB-Infrared	57.5
StitchFusion	RGB-Infrared	57.80 (+0.30)
StitchFusion+FFMs	RGB-Infrared	57.91 (+0.41)

Table 3: Comparison With State-of-the-art Results on the FMB and MFNet Dataset.

Parameter Number Efficiency

To highlight the efficiency of the StitchFusion module in terms of parameter number, we present the following formula for calculating the module’s parameter number P :

$$P = \sum_i \left((2rd_i + r^2) \cdot 2 \cdot C_m^2 \cdot \sum_j (depth_{i,j}) \right), \quad (17)$$

where d_i denotes the feature dimensions of input and output for the i -th stage, r is a hyperparameter that adjusts StitchFusion’s downsampling dimensions (set to 8 in this paper), m represents the number of modalities, and $depth_{i,j}$ indicates the depth of the backbone network for the i -th stage, C_m^2 represents the number of combinations when choosing 2 encoders to perform information-sharing out of m distinct modalities.

Table 4 demonstrates that StitchFusion achieves significant accuracy improvements with minimal increases in parameters compared to state-of-the-art methods on the DeLiVER and Mcubes datasets. For the DeLiVER dataset, StitchFusion models show accuracy gains ranging from 8.55% to 10.83% with only a 0.14M to 0.71M increase in parameters. For instance, StitchFusion-RGB-DEL achieves a 10.83 accuracy improvement with just a 2.75% increase in parameters. Similarly, on the Mcubes dataset, accuracy improvements range from 0.81% to 1.38%, while parameter increases are between 0.40M and 2.37M.

Ablation Experiment

Comparison of different modal combinations. The Table 5 provides a mIoU comparison for various modality combinations on the MCubeS dataset. As the number of modalities increases, the model’s segmentation performance gradually improves. The StitchFusion method showed a mIoU of 51.25% with the RGB-D modality, 52.08% with the

Model-Modality	Params (M)	Acc. (%)
DeLiVER Dataset		
SegFormer-RGB	25.79	57.20
CMNeXt-RGB-D	58.69	63.58
CMNeXt-RGB-DE	58.72	64.44
CMNeXt-RGB-DEL	58.73	63.30
StitchFusion-RGB-D	25.93 (+0.14)	65.75 (+8.55)
StitchFusion-RGB-DE	26.22 (+0.43)	66.03 (+8.83)
StitchFusion-RGB-DEL	26.50 (+0.71)	68.18 (+10.83)
Mcubes Dataset		
MMSFormer-RGB-A	64.88	51.30
MMSFormer-RGB-AD	65.27	52.03
MMSFormer-RGB-ADN	65.65	53.11
StitchFusion-RGB-A	65.28 (+0.40)	52.68 (+1.38)
StitchFusion-RGB-AD	66.45 (+1.18)	53.26 (+1.23)
StitchFusion-RGB-ADN	68.02 (+2.37)	53.92 (+0.81)

Table 4: Comparison of Parameters and Accuracy With SOTA Methods On DeLiVER and Mcubes Dataset.

RGB-A modality, and 52.52% with the RGB-A-D modality. Integrating StitchFusion with FFMs leads to even higher mIoU scores, with notable improvements across all tested modality groups. When StitchFusion was combined with FFMs, performance improved across all modality combinations.

Methods	Modalities	mIoU (%)
StitchFusion	RGB-N	51.67
StitchFusion	RGB-D	51.25
StitchFusion	RGB-A	52.08
StitchFusion	RGB-A-D	52.52
StitchFusion	RGB-A-D-N	<u>51.74</u>
StitchFusion+FFMs	RGB-N	53.21
StitchFusion+FFMs	RGB-D	52.72
StitchFusion+FFMs	RGB-A	52.68
StitchFusion+FFMs	RGB-A-D	<u>53.26</u>
StitchFusion+FFMs	RGB-A-D-N	53.92

Table 5: Mean IoU comparison on Modalities Combinations On MCubeS dataset.

Exploration of connection density for different StitchFusion Table 6 show that well-timed StitchFusion configurations, particularly when combined with FFMs, significantly enhance performance. In the MCubeS dataset, StitchFusion+FFMs achieves the highest mIoU of 53.92%, outperforming simpler configurations like StitchFusion(shared) and StitchFusion(ADD). Similarly, in the FMB dataset, StitchFusion(TWO, after)+FFMs leads with a mIoU of 64.85%, demonstrating the importance of both density and timing in feature fusion for optimal multimodal semantic segmentation performance.

StitchFusion is compatible with existing Feature Fusion Modules. The combination (Fig. 4 and Table 7) of StitchFusion and FFMs consistently improves performance across various experimental settings, demonstrating their complementary strengths in enhancing semantic segmentation. For

Methods	mIoU (%)	Methods	mIoU (%)
Mcubes Dataset		FMB Dataset	
sStitchFusion	51.50	StitchFusion	63.30
StitchFusion [†]	51.22	StitchFusion*	62.28
StitchFusion	51.70	tuStitchFusion	62.82
tuStitchFusion	51.12	tuStitchFusion*	62.64
sSF+FFMs	51.94	SF+FFMs	64.32
SF [†] +FFMs	52.14	SF*+FFMs	64.51
SF+FFMs	53.92	tuSF+FFMs	63.25
tuSF+FFMs	51.89	tuSF*+FFMs	64.85

Table 6: Comparison of StitchFusion’s Different Levels of Dense Connectivity on Mcubes and FMB Datasets. [†]denotes performing a pixel-wise summation of modalities other than RGB to create a new modality input. * denotes the Multi-Adapter is used in the latter two stages. SF stands for StitchFusion.

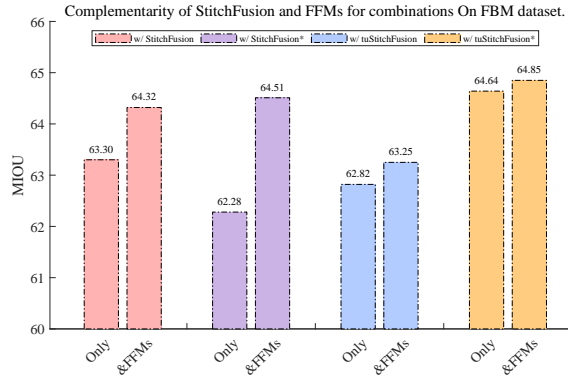


Figure 4: Complementarity of StitchFusion and FFMs for combinations On FMB dataset.

instance, on the FMB dataset, the integration of tuStitchFusion* with FFMs achieves a mIoU score of 64.85%, compared to 62.64% with tuStitchFusion* alone. Similarly, on the MFNet dataset, the combination of StitchFusion and FFMs results in a mIoU of 57.91%, slightly higher than the 57.8% from using StitchFusion alone. These specific improvements illustrate that the combined approach leverages the unique advantages of both methods to effectively handle multimodal information.

Model	MFNet (%)	PST900 (%)
StitchFusion	57.80	84.70
StitchFusion+FFMs	57.91 \uparrow	85.35 \uparrow
StitchFusion*	57.76	83.41
StitchFusion*+FFMs	58.13 \uparrow	85.31 \uparrow

Table 7: Complementarity of StitchFusion and FFMs for combinations on MFNet and PST900 dataset. * denotes the MultiAdapter is used in the latter two stages.

Semantic Segmentation Visualization

t-SNE visualization. The t-SNE visualization in Fig. 5 demonstrates the clustering of features extracted by Stitch-

Fusion on the DeLiVER dataset. As the number of modalities increases from RGB to RGBE, RGBDE, and RGBDEL, the clusters become more distinct and well-separated, indicating enhanced feature differentiation. This suggests that incorporating additional modalities improves the model’s ability to learn more discriminative features.

Segmentation Visualizations. The segmentation visualizations in Fig. 6 highlight the effectiveness of StitchFusion on the Mcubes dataset and DeLiVR dataset. With more modalities (RGBA, RGBD, RGBN, RGBAD, RGBADN), the segmentation results become progressively more accurate and detailed. As marked by the box, the boundaries of different segments are clearer, and the segmentation maps more closely resemble the ground truth images. This demonstrates that incorporating additional modalities enables the model to capture more comprehensive information, resulting in improved segmentation performance.

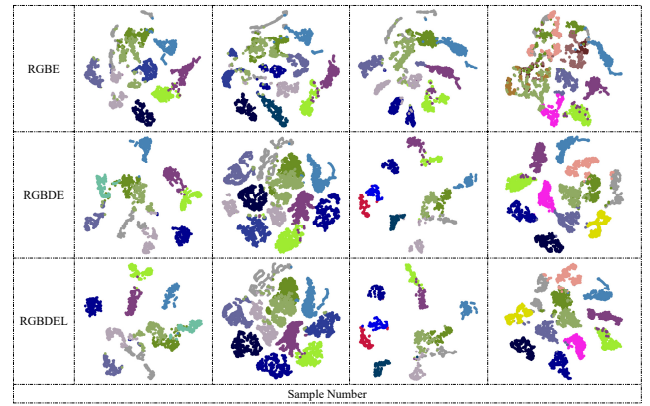


Figure 5: t-SNE Visualization of StitchFusion On DeLiVER Dataset.

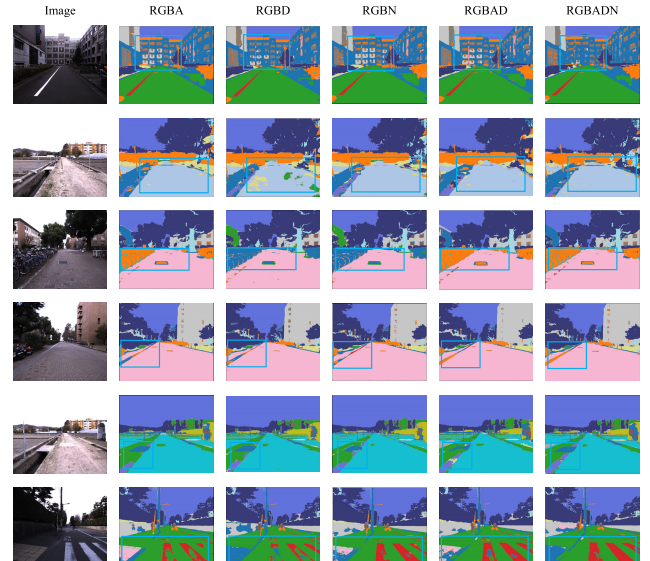


Figure 6: Visulization of StitchFusion On Mcubes Dataset.

Conclusion

This paper introduces StitchFusion, a novel approach designed to enhance feature fusion and alignment between multiple visual features for semantic segmentation. Our method progressively selects and fuses relevant features, improving model accuracy and robustness across various image recognition scenarios. Through extensive experiments, we demonstrate that StitchFusion outperforms existing methods, highlighting its capability to effectively handle complex image recognition challenges. However, the MultiAdapter is designed as a simple MLP architecture, which may not be efficient enough for fine-grained feature processing and sharing. In the future, the MultiAdapter requires a more suitable and fine-grained design.

Appendices

Supplementary Visualization of StitchFusion

In this appendix, we provide a comprehensive set of visualizations and analyses to elucidate the performance and capabilities of the StitchFusion method. Fig. 7 offers a detailed visualization of the segmentation results on the DeLiVER dataset, showcasing the method’s precision in delineating boundaries and preserving fine details. To further underscore the method’s feature extraction ability, Fig. 8 employs t-SNE to project the high-dimensional feature representations onto a two-dimensional plane. The distinct clusters in the t-SNE plots indicate the method’s ability to capture and separate the nuances within the data. Fig. 10 extends the

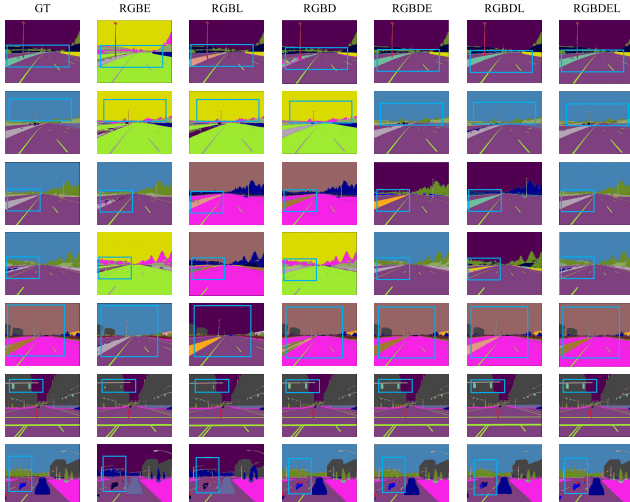


Figure 7: Visulization of StitchFusion On DeLiVER Dataset.

qualitative assessment of the Mcubes dataset by presenting additional segmentation results, thereby demonstrating the model’s adaptability across varied data environments. Finally, Fig. 9 provides more visualizations of StitchFusion’s segmentation outcomes on the DeLiVER dataset, offering a broader perspective on the model’s performance. These additional images may include comparative analyses with

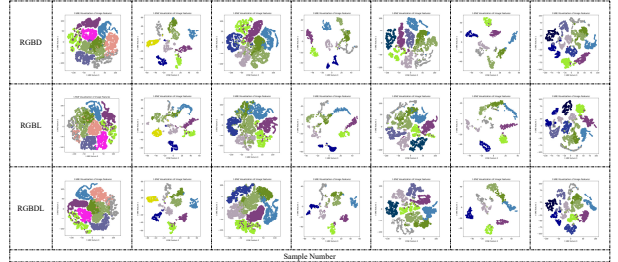


Figure 8: t-SNE Visualization On DeLiVER Dataset.

other methods or highlight the method’s efficacy in handling complex or challenging segments within the dataset.

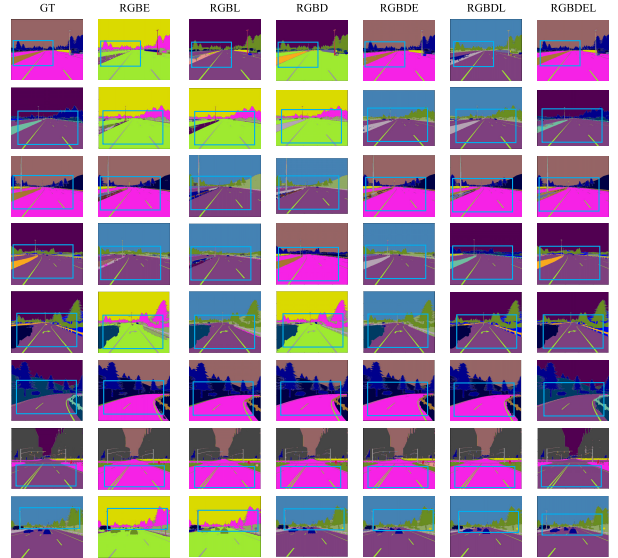


Figure 9: Supplementary Visualization On DeLiVER Dataset.

Per-class Comparision with State-of-the-art Models

In our analysis, we present a comparative study of segmentation performance across different categories and datasets, focusing on the DeLiVER dataset and various modality combinations shown on the left side of Fig. 11. Additionally, we compare the per-class mIOU performance on the Mcubes (Fig. 11 right), FBM (Fig. 8), and MFNet (Fig. 9) datasets. The results reveal distinct advantages and limitations of each method in handling diverse categories. For instance, while some methods excel in categories such as "Sky" and "Truck," they may underperform in more challenging categories like "Human" and "Plaster." Our proposed method, StitchFusion+FFMs, demonstrates balanced and robust performance across categories, achieving high mIOU scores in previously challenging areas. This comprehensive analysis not only highlights the strengths and weaknesses of each method but also provides valuable insights into their applicability across different datasets and categories, guiding further improvements in segmentation techniques.

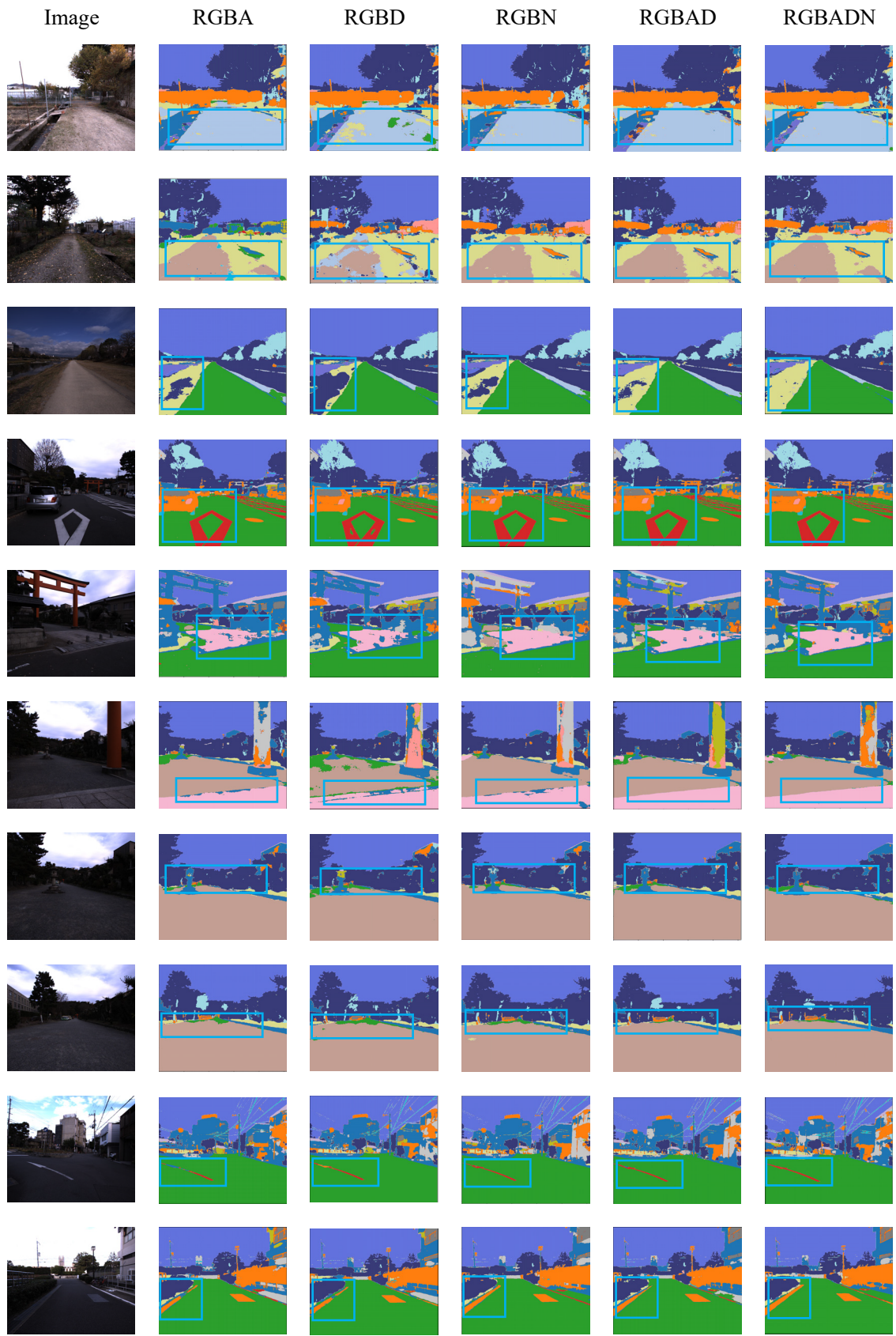


Figure 10: Supplementary Visualization of StitchFusion On Mcubes Dataset.

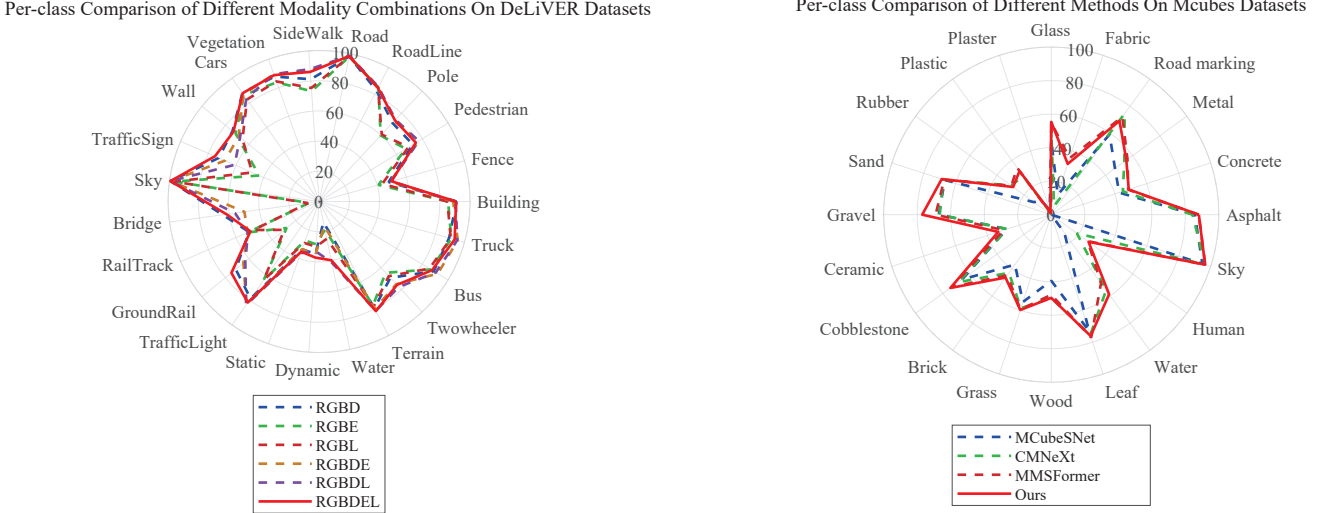


Figure 11: Per-class IoU (%) comparison on DeLiVER dataset and Mcubes Dataset. The main comparative data come from the article (Zhang et al. 2023b).

Methods	Car	Person	Truck	T-Lamp	T-Sign	Building	Vegetation	Pole	mIoU(%)
GMNet	79.3	60.1	22.2	21.6	69.0	79.1	83.8	39.8	49.2
LASNet	72.6	48.6	14.8	2.9	59.0	75.4	81.6	36.7	42.5
EGFNet	77.4	63.0	17.1	25.2	66.6	77.2	83.5	41.5	47.3
FEANet	73.9	60.7	32.3	13.5	55.6	79.4	81.2	36.8	46.6
DIDFuse	77.7	64.4	28.8	29.2	64.4	78.4	82.4	41.8	50.6
ReCoNet	75.9	65.8	14.9	34.7	66.6	79.2	81.3	44.9	50.9
U2Fusion	76.6	61.9	14.4	28.3	68.9	78.8	82.2	42.2	47.9
TarDAL	74.2	56.0	18.8	29.6	66.5	79.1	81.7	41.9	47.9
SegMiF	78.3	65.4	47.3	43.1	74.8	82.0	85.0	49.8	54.8
MMSFormer	82.6	69.8	<u>44.6</u>	<u>45.2</u>	<u>79.7</u>	83.0	<u>87.3</u>	<u>51.4</u>	61.7
StitchFusion	83.3	75.1	42.8	38.7	78.9	85.1	88.5	52.1	<u>63.3</u>
StitchFusion+FFMs	<u>83.0</u>	73.0	42.6	52.0	80.4	<u>83.6</u>	88.5	49.5	64.3

Table 8: Per-class mIoU (%) comparison on FMB dataset for RGB-infrared modalities. The main comparative data come from the article (Kaykobad and et al. 2023).

Method	Unlabeled	Car	Person	Bike	Curve	Car Stop	Guardrail	Color Cone	Bump	mIoU (%)
MFNet	96.9	65.9	58.9	42.9	29.9	9.9	0.0	25.2	27.7	39.7
SA-Gate	96.8	73.8	59.2	51.3	38.4	19.3	0.0	24.5	48.8	45.8
Depth-aware CNN	96.9	77.0	53.4	56.5	30.9	29.3	8.5	30.1	32.4	46.1
ACNet	96.7	79.4	64.7	52.7	32.9	28.4	0.8	16.9	44.4	46.3
PSTNet	97.0	76.8	52.6	55.3	29.6	25.1	15.1	39.4	45.0	48.4
RTFNet	98.5	87.4	70.3	62.7	45.3	29.7	2.0	29.1	55.7	53.2
FuseSeg	97.6	80.7	61.0	66.4	44.8	22.7	6.4	46.9	47.9	54.5
AFNet	98.0	86.0	67.4	62.6	37.5	28.9	4.6	47.4	50.0	53.6
ABMDRNet	98.6	84.8	69.6	60.7	33.1	33.3	5.1	47.4	50.3	54.8
FEANet	97.3	87.8	71.1	61.1	46.5	22.1	9.5	49.3	46.4	55.3
DHIFNet	97.7	87.7	67.1	63.4	39.5	42.4	9.5	49.3	<u>56.0</u>	57.3
GMNet	97.5	86.5	73.1	61.7	41.4	19.3	<u>14.5</u>	48.7	48.8	57.3
StitchFusion	98.3	89.5	75.1	65.6	47.9	<u>32.8</u>	0.5	57.2	53.4	57.8
StitchFusion+FFMs	98.3	89.7	75.1	<u>66.1</u>	<u>45.7</u>	28.3	8.1	<u>52.9</u>	57.0	57.9

Table 9: Per-class results on MFNet dataset for RGB-Thermal segmentation. The main comparative data come from the article (Dong et al. 2023).

References

Badrinarayanan, V.; Kendall, A.; and Cipolla, R. 2017. Segnet: A deep convolutional encoder-decoder architecture for image segmentation. *IEEE transactions on pattern analysis and machine intelligence*, 39(12): 2481–2495.

Cao, B.; Guo, J.; Zhu, P.; and Hu, Q. 2024. Bi-directional adapter for multimodal tracking. In *Proceedings of the AAAI Conference on Artificial Intelligence*, volume 38, 927–935.

Chen, J.; Wang, X.; Guo, Z.; Zhang, X.; and Sun, J. 2021. Dynamic region-aware convolution. In *Proceedings of the IEEE/CVF conference on computer vision and pattern recognition*, 8064–8073.

Chen, L.-C.; Papandreou, G.; Schroff, F.; and Adam, H. 2017. Rethinking atrous convolution for semantic image segmentation. *arXiv preprint arXiv:1706.05587*.

Chen, L.-C.; Zhu, Y.; Papandreou, G.; Schroff, F.; and Adam, H. 2018. Encoder-decoder with atrous separable convolution for semantic image segmentation. In *Proceedings of the European conference on computer vision (ECCV)*, 801–818.

Dong, S.; Zhou, W.; Xu, C.; and Yan, W. 2023. EGFNet: Edge-aware guidance fusion network for RGB–thermal urban scene parsing. *IEEE Transactions on Intelligent Transportation Systems*.

Dosovitskiy, A.; Beyer, L.; Kolesnikov, A.; Weissenborn, D.; Zhai, X.; Unterthiner, T.; Dehghani, M.; Minderer, M.; Heigold, G.; Gelly, S.; et al. 2020. An image is worth 16x16 words: Transformers for image recognition at scale. *arXiv preprint arXiv:2010.11929*.

Fu, J.; Liu, J.; Tian, H.; Li, Y.; Bao, Y.; Fang, Z.; and Lu, H. 2019. Dual attention network for scene segmentation. In *Proceedings of the IEEE/CVF conference on computer vision and pattern recognition*, 3146–3154.

Ha, Q.; Watanabe, K.; Karasawa, T.; Ushiku, Y.; and Harada, T. 2017. MFNet: Towards real-time semantic segmentation for autonomous vehicles with multi-spectral scenes. In *2017 IEEE/RSJ International Conference on Intelligent Robots and Systems (IROS)*, 5108–5115. IEEE.

Hazirbas, C.; Ma, L.; Domokos, C.; and Cremers, D. 2016. Fusenet: Incorporating depth into semantic segmentation via fusion-based cnn architecture. In *Asian conference on computer vision*, 213–228. Springer.

He, Q. 2024. Prompting Multi-Modal Image Segmentation with Semantic Grouping. In *Proceedings of the AAAI Conference on Artificial Intelligence*, volume 38, 2094–2102.

Huang, Z.; Wang, X.; Huang, L.; Huang, C.; Wei, Y.; and Liu, W. 2019. Ccnet: Criss-cross attention for semantic segmentation. In *Proceedings of the IEEE/CVF international conference on computer vision*, 603–612.

Joze, H. R. V.; Shaban, A.; Iuzzolino, M. L.; and Koishida, K. 2020. MMTM: Multimodal transfer module for CNN fusion. In *Proceedings of the IEEE/CVF conference on computer vision and pattern recognition*, 13289–13299.

Kaykobad, M. R.; and et al. 2023. Multimodal Transformer for Material Segmentation. *arXiv e-prints*, arXiv–2309.

Liang, Y.; Wakaki, R.; Nobuhara, S.; and Nishino, K. 2022. Multimodal material segmentation. In *Proceedings of the IEEE/CVF Conference on Computer Vision and Pattern Recognition*, 19800–19808.

Liu, J.; Liu, Z.; Wu, G.; Ma, L.; Liu, R.; Zhong, W.; Luo, Z.; and Fan, X. 2023. Multi-interactive feature learning and a full-time multi-modality benchmark for image fusion and segmentation. In *Proceedings of the IEEE/CVF international conference on computer vision*, 8115–8124.

Liu, Z.; Lin, Y.; Cao, Y.; Hu, H.; Wei, Y.; Zhang, Z.; Lin, S.; and Guo, B. 2021. Swin transformer: Hierarchical vision transformer using shifted windows. In *Proceedings of the IEEE/CVF International Conference on Computer Vision*, 10012–10022.

Long, J.; Shelhamer, E.; and Darrell, T. 2015. Fully convolutional networks for semantic segmentation. In *Proceedings of the IEEE conference on computer vision and pattern recognition*, 3431–3440.

Ronneberger, O.; Fischer, P.; and Brox, T. 2015. U-net: Convolutional networks for biomedical image segmentation. In *International Conference on Medical image computing and computer-assisted intervention*, 234–241. Springer.

Shivakumar, S. S.; Rodrigues, N.; Zhou, A.; Miller, I. D.; Kumar, V.; and Taylor, C. J. 2020. Pst900: Rgb-thermal calibration, dataset and segmentation network. In *2020 IEEE international conference on robotics and automation (ICRA)*, 9441–9447. IEEE.

Xie, E.; Wang, W.; Yu, Z.; Anandkumar, A.; Alvarez, J. M.; and Luo, P. 2021. SegFormer: Simple and efficient design for semantic segmentation with transformers. volume 34, 12077–12090.

Zhang, J.; Liu, H.; Yang, K.; Hu, X.; Liu, R.; and Stiefelhagen, R. 2023a. CMX: Cross-modal fusion for RGB-X semantic segmentation with transformers. *IEEE Transactions on Intelligent Transportation Systems*.

Zhang, J.; Liu, R.; Shi, H.; Yang, K.; Reiß, S.; Peng, K.; Fu, H.; Wang, K.; and Stiefelhagen, R. 2023b. Delivering arbitrary-modal semantic segmentation. In *Proceedings of the IEEE/CVF Conference on Computer Vision and Pattern Recognition*, 1136–1147.

Zhao, H.; Shi, J.; Qi, X.; Wang, X.; and Jia, J. 2017. Pyramid scene parsing network. In *Proceedings of the IEEE conference on computer vision and pattern recognition*, 2881–2890.

Zheng, S.; Lu, J.; Zhao, H.; Zhu, X.; Luo, Z.; Wang, Y.; Fu, Y.; Feng, J.; Xiang, T.; Torr, P. H.; et al. 2021. Rethinking semantic segmentation from a sequence-to-sequence perspective with transformers. In *Proceedings of the IEEE/CVF Conference on Computer Vision and Pattern Recognition*, 6881–6890.

Zhou, W.; Dong, S.; Fang, M.; and Yu, L. 2023. CACFNet: Cross-modal attention cascaded fusion network for RGB-T urban scene parsing. *IEEE Transactions on Intelligent Vehicles*.

Zhou, W.; Liu, J.; Lei, J.; Yu, L.; and Hwang, J.-N. 2021. GMNet: Graded-feature multilabel-learning network

for RGB-thermal urban scene semantic segmentation. *IEEE Transactions on Image Processing*, 30: 7790–7802.